Synthesis and electromagnetic properties of NH$_2$-MIL-88B(Fe) crystals with morphology and size controllable through synergistic effects of surfactant and water

Jieling Liu[1], Jiaji Yang[1], Shuyue An[1], Meiqi Wen[1], Xian Wang[1], Rongzhou Gong[1], and Yan Nie[1,*] (ID)

[1] School of Optical and Electronic Information, Huazhong University of Science and Technology, Wuhan 430074, People's Republic of China

ABSTRACT

Metal-organic framework (MOF) crystals have promising applications in a number of different fields, but the growth of MOF crystals with controllable morphology and high uniformity remains a major challenge. By taking the advantage of the synergistic effects of water molecules in the mixed solvent and polyvinylpyrrolidone (PVP) surfactants, this work demonstrates an approach for the preparation of NH$_2$-MIL-88B(Fe) MOF crystals with both highly customizable size and aspect ratios and high uniformity. The effects of the concentration of water in the mixed solvent and the amount of PVP surfactants on the morphology and size of the MOF crystals were investigated. The morphology and crystalline properties were characterized by scanning electron microscopy and X-ray diffraction techniques. The data showed that through controlling the concentration of water in the solvent and the amount of the PVP surfactant, the size of the MOF crystals can be tuned rather widely, over 344–5.14 μm, while the aspect ratio of the crystals can be varied widely over 1.0–7.1. Possible mechanisms for such high tunability were discussed. As an example of potential applications, the complex permeability and permittivity of MOF-derived composites (25 wt%) were measured over a wide frequency range of 2–18 GHz. The parameters were then used to evaluate the potential for electromagnetic wave absorption. The results indicate that the composite with a thickness of only 1.2 mm exhibits a "− 10 dB" absorption bandwidth of 4.1 GHz and a minimum reflection of − 20 dB. Such bandwidth and reflection properties provide inspiration for future design of lightweight, broadband electromagnetic wave absorbers from the perspective of fine morphology control.

Address correspondence to E-mail: nieyan@hust.edu.cn

1 Introduction

Metal-organic frameworks (MOFs) are a kind of emerging materials with porous network structures that are composed of central metal ions as nodes and organic ligands as bridging components [1]. In recent years, MOFs have received more and more attention thanks to the almost infinite possibilities of combinations of metals and ligands. Such infinite combination possibilities offer a high degree of tunability in both the size and morphology of MOFs and thereby make the physical and chemical properties of MOF materials highly customizable [2–5]. In terms of practical applications, MOFs can be used in a wide range of fields that include gas storage [6, 7], gas and liquid separation [8, 9], catalysis [10, 11], medicine [12, 13], environmental remediation [14], and electromagnetic wave absorption [15].

The size, aspect ratio, and uniformity of MOF crystals play important roles in practical applications. For example, for medical imaging, the size and aspect ratio of MOF crystals largely affect the imaging resolution [16]. For the use of ZIF-7-III as a filler in mixed-matrix membranes, the particle aspect ratio is an important factor, because high aspect ratio fillers effectively hinder the permeation of non-permeable gas species, which increases the selectivity of the membrane when the fillers are aligned perpendicular to the gas flow direction [17, 18]. Further, it has been previously shown that MOF crystals with large aspect ratios and low defect concentration can notably enhance charge and mass transfer when they are used for gas separation [19].

The choice of the synthesis method is very important for the preparation of MOF materials; it affects both the structure and properties of the product. Several different methods have been developed to synthesize MOFs. These methods include the sonochemical method [20], microwave-assisted synthesis [21, 22], mechanochemical synthesis [23], surfactant-assisted synthesis [22, 24], position modulation [25, 26], and the solvothermal method [27]. Although there are a good number of different synthetic approaches, the precise control of the size and aspect ratio of MOF materials remains a major challenge. For example, for the microwave-assisted method, the complex spatial distribution of the microwave field can cause the microwave reactor to generate hot spots and thereby result in local overheating; such local overheating makes MOFs deteriorate into irregular

geometric shapes [28]. For the mechanochemical synthesis approach, it is not easy to tune the size and shape of the obtained MOF crystals.

Among the above-mentioned approaches, the solvothermal method has been a very popular one, but the obtained MOF crystals often have non-uniform size distribution [29, 30]. The solvothermal method has the advantages of simple operating process, high product purity, and good crystallinity, which are important for the synthesis of bio-inspired materials for applications in bioscience and the preparation of nanostructured particles in nanotechnology. [31–35]. In order to better control the size (and the aspect ratio) of MOF materials, several new approaches have been proposed and explored. One method is to introduce surfactants into the reaction system. Because the surfactant molecules can be weakly coordinated with metal ions, the surfactant provides steric stability for the nucleation growth of MOF crystals, slows down the nucleation rate, and therefore enables easy control of the crystal size [36]. For example, a previous work on the synthesis of Fe-MIL-88B-NH_2 crystals has used non-ionic triblock copolymer F127 and acetic acid as the stabilizer and the deprotonation agent, respectively, to better control the size and shape of the crystals [37]. In another work, Cai et al. introduced polyvinylpyrrolidone (PVP) as a surfactant into the reaction medium to adjust the size and morphology of Fe-MIL-88B [24]. In addition to the surfactant, the solvent is also a key tuning element in the synthesis of MOFs; the properties of the solvent, such as the polarity and solubility of structural units, greatly affect the nucleation and growth of MOF materials [2]. For example, Cheng et al. prepared NH_2-MIL-53(Al) crystals with controllable size and morphology by changing the ratio of water in the N,N'-dimethylformamide (DMF) -water mixed solvent system [38].

This article reports on the preparation of NH_2-MIL-88B(Fe) MOF crystals with controllable crystal size and aspect ratios using the solvothermal method. The high controllability of the crystal morphology and size is achieved through the integration of the above-mentioned surfactant and solvent approaches. Specifically, through the control of the PVP surfactant and the water concentration in the DMF/water solvent, the size of the NH_2-MIL-88B(Fe) crystal can be tuned over a wide range of 0.34–5.14 μm, while the aspect ratio of the crystal can be varied in a wide range of 1.0–7.1. The prepared NH_2-MIL-88B(Fe)

crystals have potential applications in gas storage and separation, drug delivery, and electromagnetic wave absorption. As one example, the potential application of NH_2-MIL-88B(Fe) crystals in electromagnetic wave absorption was investigated.

2 Experimental details

2.1 Materials

Ferric chloride ($FeCl_3$, 97%, Sigma-Aldrich), H_2N-BDC ($C_8H_7NO_4$, 98%, Aladdin), polyvinylpyrrolidone (PVP, MW = 40,000, Sigma-Aldrich), N,N'-dimethylformamide (DMF, 99.8%), and anhydrous ethanol were obtained from Sinopharm Chemical Reagent Co. Ltd. All of the chemicals and solvents were used as received without any further purification.

2.2 Preparation of NH_2-MIL-88B(Fe)

The NH_2-MIL-88B(Fe) crystals were prepared through a facile solvothermal process that is similar to the process reported previously, but with some slight modifications [16, 24, 37]. A precursor solution was prepared by mixing $FeCl_3$ (300 mg, 1.849 mmol), H_2N-BDC (1100 mg, 6.072 mmol), and 0–16 g of PVP (0 g, 2 g, 4 g, 8 g, 16 g) in a solution (73 mL) of DMF and water. The mixture solution was transferred into a 100-mL-Teflon autoclave for solvothermal treatment at a temperature of 115 °C for a time period of 3 h. The products were collected by centrifugation first and were then washed several times with anhydrous ethanol and DMF. After that, the products were dried in an oven at a temperature of 60 °C for a time period of 12 h.

2.3 Preparation of sample MIL-A

The samples synthesized under the conditions of a fixed PVP amount of 16 g and a volume percentage of water in the mixed solvent of 45 vol% were annealed in a tube furnace under nitrogen flow at 800 °C for a period of 2 h. The heating rate was 10 °C min^{-1}. The obtained products were denoted as "sample MIL-A."

2.4 Characterization

The composition and crystalline structure of the samples were characterized by X-ray powder diffraction (XRD) techniques, using an Empyrean XRD system (PANalytical B.V.) with Cu K radiation (λ = 0.15406 nm, 40 kV, 40 mA). The morphology and microstructures of the samples were characterized by a field emission scanning electron microscope (FESEM, GeminiSEM 300, Zeiss). The electromagnetic properties of the samples were measured by a vector network analyzer (VNA, E5071c, Agilent) over a wide frequency range of 2–18 GHz. This involved the measurements of scattering parameters of the samples and the calculation of the relative permeability (μ_r) and relative permittivity (ε_r) from the measured scattering parameters, using the software "Agilent Technologies 85071" [39–41]. The electromagnetic measurements made use of a ring-type sample that was prepared as follows: The MOF materials were first mixed uniformly with paraffin wax with a mass ratio of 25%; the mixture was then pressed into a ring shape with an outer diameter of 7.0 mm, an inner diameter of 3.04 mm, and a thickness of 2.50 ± 0.1 mm.

3 Results and discussions

3.1 Influences of DMF-water mixed solvent ratio on morphology and size

A series of NH_2-MIL-88B(Fe) MOF crystals with different sizes and morphologies were prepared by varying the volume fraction of deionized water in the DMF-water mixed solvents while keeping all other reaction conditions constant. Figure 1 shows the SEM images of six MOF samples prepared with different water volume fractions, as indicated in the figure caption. As shown in Fig. 1a, when pure DMF was used as a solvent, the product resulted was many crystal aggregates that consisted of numerous small MOF crystals; such aggregation resulted from the relatively high surface energy of the small MOF crystals [24]. When a small amount of water was added to the mixed solvent (water ratio = 4 vol%), the obtained sample remained as some crystal aggregates, but some small crystals exhibit octahedral morphology, as can be seen in Fig. 1b. However, when the volume fraction of the water was increased to 25 vol%, the product changed from crystal aggregates into monocrystals with spindle-like morphology, as can be seen in Fig. 1c. The average length of the crystals is less than 300 nm. When the ratio of the water was further increased to 50 vol%, the resulting
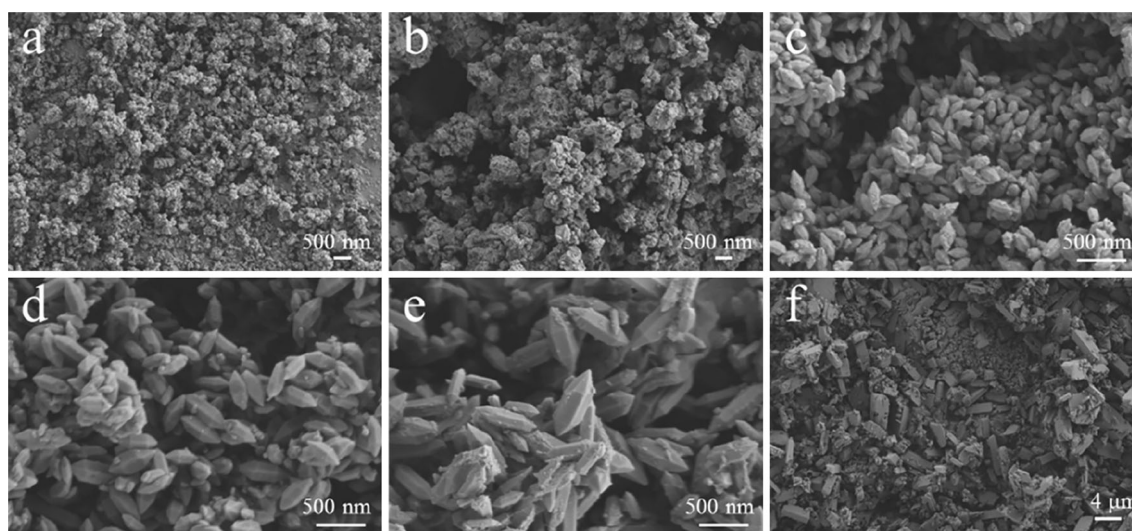
Fig. 1 Scanning electron microscopy (SEM) images of NH_2-MIL-88B(Fe) crystals prepared with different volume fractions (x) of water in the mixed DMF-water solvent: **a** $x = 0$ vol%, **b** $x = 4$ vol%, **c** $x = 25$ vol%, **d** $x = 50$ vol%, **e** $x = 75$ vol%, and **f** $x = 100$ vol%

crystals remained the spindle shape, though there exist a small number of small crystals on the large crystals, as shown in Fig. 1d. The average length of the large crystals is about 450 nm. With a further increase in the fraction of the water to 75 vol%, the morphology of the product became less uniform, and the average length of the large crystals further increased to over 700 nm. This can be clearly seen in Fig. 1e. In the case of 100 vol% water as the solvent, the morphology of the resulting product was irregular rod-shaped, as shown in Fig. 1f.

To summarize briefly, the SEM images in Fig. 1 clearly show that the water ratio in the solvent mixture played critical roles in the size and morphology of the synthesized NH_2-MIL-88B(Fe) crystals. As the water ratio increases from 0 to 75 vol%, the crystal aggregate of NH_2-MIL-88B(Fe) dispersed to small monocrystals with spindle shape first, and then the monocrystals gradually increased their size. As the ratio of the water continued to increase to 100 vol% (namely, the solvent became pure water), the average size of the crystals continued to increase, but the crystal morphology evolved from spindle shape to irregular rod shape. As such, one can tentatively speculate that water may promote the growth of crystals in a specific direction. However, it seems that it is difficult to control the morphological uniformity of the product only through controlling the content of water in the mixed solvent.

It is known that in general, the faster the nucleation rate during the crystal growth of MOFs is, the smaller the size of the resulting MOF crystals is, and vice versa [25]. During the preparation of MOF crystals, the solvent can change the deprotonation rate of the organic linkers and affect the coordination interaction between organic linkers and the metal ions, thereby controlling the nucleation and crystal growth rates; this makes possible the preparation of MOF crystals with tunable size and morphology [38]. Therefore, it can be deduced that the above-presented dramatic change in the crystal size and morphology of NH_2-MIL-88B(Fe) is to some extent related to the degree of deprotonation of NH_2-BDC in the mixed solvent system. To verify this deduction, the pH values of three kinds of mixtures were measured, with the results presented in Table 1. In the table, R denotes the volume ratio of water in the mixed solvents, pH_1 and pH_2 represent the pH values when only NH_2-BDC or $FeCl_3$ is added to the mixed solvents, respectively, and pH_3 represents the pH values of the reaction mixtures before crystallization. The values of pH_1 indicate that the pH value of the solution

Table 1 pH values of the reaction mixtures before crystallization

Mixed solution	a	b	c	d	e	f
R/vol%	0	4	25	50	75	100
pH_1	6.5	4.5	4.1	3.3	3.5	3.8
pH_2	3.1	3.0	3.0	3.0	2.9	2.9
pH_3	3.0	2.9	2.5	2.7	3.0	3.2

decreases rapidly from 6.5 to 3.3 when the water ratio is increased from 0% to 50%. However, as the water ratio continues to increase to 100 vol%, the pH value gradually increases to 3.8. The rapid decrease of the pH value from 6.5 to 3.3 is probably because the interspersion of water molecules among NH_2-BDC molecules reduces the association effect between them. The weaker association effect makes the deprotonation of NH_2-BDC molecules easier and thereby produces more hydrogen protons, leading to a drop in the pH value. Moreover, DMF molecules are more likely to form weak coordination with hydrogen protons than water molecules and therefore have a stronger ability to enhance the deprotonation of NH_2-BDC than water. Thus, the deprotonation of the organic linkers was inhibited when the ratio of water in the mixed solvent was increased. At the same time, the solubility of NH_2-BDC is reduced with the increase of the water ratio in the mixed solvents, which leads to a decrease in the number of dissolved NH_2-BDC molecules in the solution and a decrease in the number of hydrogen protons produced [38]. These facts together result in a gradual increase in the pH value of the solution.

It can be seen from Table 1 that the pH_2 value remains almost unchanged, and the overall value is lower than the pH_1 value. Therefore, it can be considered that the change of pH_3 is mainly caused by the deprotonation of NH_2-BDC in the mixed solution. Also, it should be noted that the pH_2 values are all lower than the corresponding pH_1 values, which is mainly due to the hydrolysis of $FeCl_3$. Further, one can also see that the changing trend of pH_3 was closely related to the changing pattern of the NH_2-MIL-88B(Fe) crystal size and morphology. First, when a small amount of water was added to the solvent, the pH value of the mixed solution dropped. This means that the rate of deprotonation of the organic linkers increases, and more deprotonated NH_2-BDC ions can be coordinated with the metal ions (Fe(III)), leading to a faster nucleation rate and smaller crystals. This is consistent with the small crystal size shown in the SEM image in Fig. 1b. Second, when the ratio of water in the mixed solvent continued to increase beyond 25 vol%, the pH value of the mixed solution starts to increase and the rate of deprotonation of NH_2-BDC molecules is reduced. This means that fewer NH_2-BDC ions are available for coordination with Fe(III), leading to a slower nucleation rate and a corresponding increase in the crystal size.

3.2 Effects of PVP on morphology and size

Surfactants are often used to manipulate the size and morphology of nanomaterials including MOFs [22, 24, 37]. The effect of varying the amount of the PVP surfactant on the morphology of iron-based MOFs was investigated by keeping the water ratio of the mixed solvent constant at 25 vol% during the preparation process. Figure 2 shows the SEM images of the samples prepared by adding different masses of the PVP. First, from the perspective of the effects of the PVP on the size of iron-based MOF crystals, it can be seen that the crystal length of the obtained samples shows an increasing trend with the increase of the PVP addition. If Fig. 2b is compared with Fig. 2a for the sample without the PVP, it is very clear that when a small amount of the PVP (1 g) was added, the average length of the crystals increased dramatically from 270 ± 20 nm to 4.0 ± 0.2 μm, the average width of the crystals increased from 120 ± 10 to 1.55 ± 0.1 μm, and the aspect ratio increased from about 2.3 to 2.6. As the mass of the PVP added was increased to 16 g, the average length of the crystals further increased to 6.8 ± 0.2 μm, the average width increased to 2.37 ± 0.1 μm, and the aspect ratio increased to about 2.8.

Second, the images in Fig. 2 also indicate that the PVP addition also affects the morphology of the products. Specifically, when the PVP mass was increased, the morphology of the crystals evolved from spindle-like particles to bipyramidal hexagonal prisms. This is because the PVP molecule may be oriented along the [001] direction, which interacts much more strongly with the {010} crystal facets than with the {011} facets of the MOF materials, leading to different growth rates for the different facets. The net effect is an increase in the crystal size and an evolution of the morphology from spindle-like particles to bipyramidal hexagonal prisms [24].

Finally, it is also observed that when the addition of the PVP is less than 8 g, the small nanocrystals aggregated onto the large crystals, due to their relatively high surface energy. This resulted in the non-uniformity of the product's morphology, as shown in Fig. 2a–d. When the amount of the PVP added continued to increase from 8 to 16 g, almost no small nanocrystals were seen, and the product morphology became more uniform, as shown in Fig. 2e, f. This is because during the nucleation and crystal growth of NH_2-MIL-88B(Fe), the PVP provides steric stabilization, and its amide unit

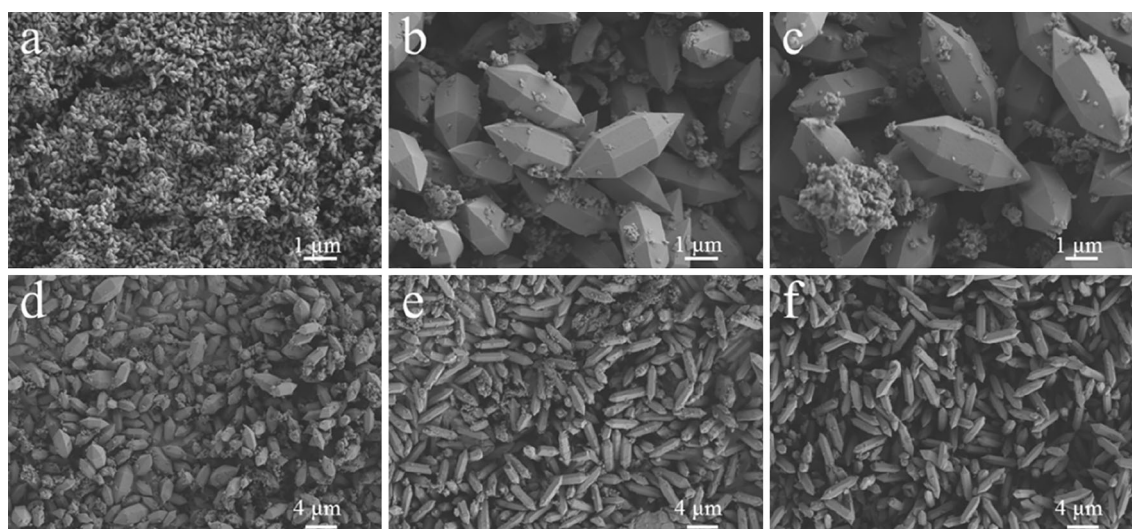**Fig. 2** SEM images of NH_2-MIL-88B(Fe) crystals prepared by keeping the water ratio of the DMF-water mixed solvent constant at 25 vol% while varying the amount of the PVP surfactant added: **a** 0 g, **b** 1 g, **c** 2 g, **d** 4 g, **e** 8 g, and **f** 16 g

coordinates periodically with Fe(III), reducing the number of the nucleation points and effectively preventing the aggregation of crystals, and thereby resulting in a more uniform product morphology [42]. However, the increase of the crystal aspect ratio due to the PVP addition during the preparation process is very limited.

3.3 Synergistic effects of water and PVP on morphology and size

The data presented above evidently indicate that (1) the water ratio in the mixed solvent can be used to effectively control and tune the crystal size and aspect ratio and (2) the amount of the PVP surfactant can be used to effectively tune the crystal size and improve the uniformity. In order to synthesize MOF crystals with both tunable crystal size and aspect ratios and high uniformity, the synergistic effects of water and PVP were investigated. Figure 3 shows the SEM images of the samples synthesized with different water ratios in mixed solvents and the addition of 16 g PVP. As shown in Fig. 3a, when the mixed solvent used is pure DMF, the crystal morphology is octahedral; the average length of the crystal is about 379 nm, the average width is about 362 nm, and the average aspect ratio is about 1.0. When a small amount of water was added to the mixed solvent (water ratio = 5 vol%), the morphology of the crystals evolved from octahedral shape to bipyramidal hexagonal prisms, as can be seen in Fig. 3b. The

average length of the crystal is about 344 nm, the average width is about 153 nm, and the average aspect ratio is now increased to 2.2. As the ratio of water was further increased to 15 vol%, the crystal morphology remained unchanged, but the average length of the crystals increased to 1.20 μm, the average width increased to 513 nm, and the average aspect ratio increased to 2.4, as shown in Fig. 3c. With a further increase in the water ratio to 25 vol%, the average length of the crystals increased to 5.14 μm, the average width increased to 1.38 μm, and the average aspect ratio further increased to as high as 3.8. These results are clearly shown in Fig. 3d. Interestingly, when the water ratio continued to increase to 35 vol%, although the morphology of the crystals did not change, the size of the crystals started to decrease, with the average length and width values decreased to 2.40 μm and 542.3 nm, respectively. However, the average aspect ratio increased to 4.4. These results are shown Fig. 3e. When the water ratio reached 45 vol%, the morphology of the crystals became slender and nano-needle-like, as can be seen in Fig. 3f. The average length of the crystals is 2.77 μm and the average width is further reduced to about 390 nm, but the average aspect ratio increased significantly to 7.1.

To better illustrate the tunability of the aspect ratio of the MOF crystals, Fig. 4 plots the aspect ratio as a function of the volume percentage of water in the mixed solvent. It is evident from the data in Fig. 4 that the aspect ratio can be tuned over a really wide
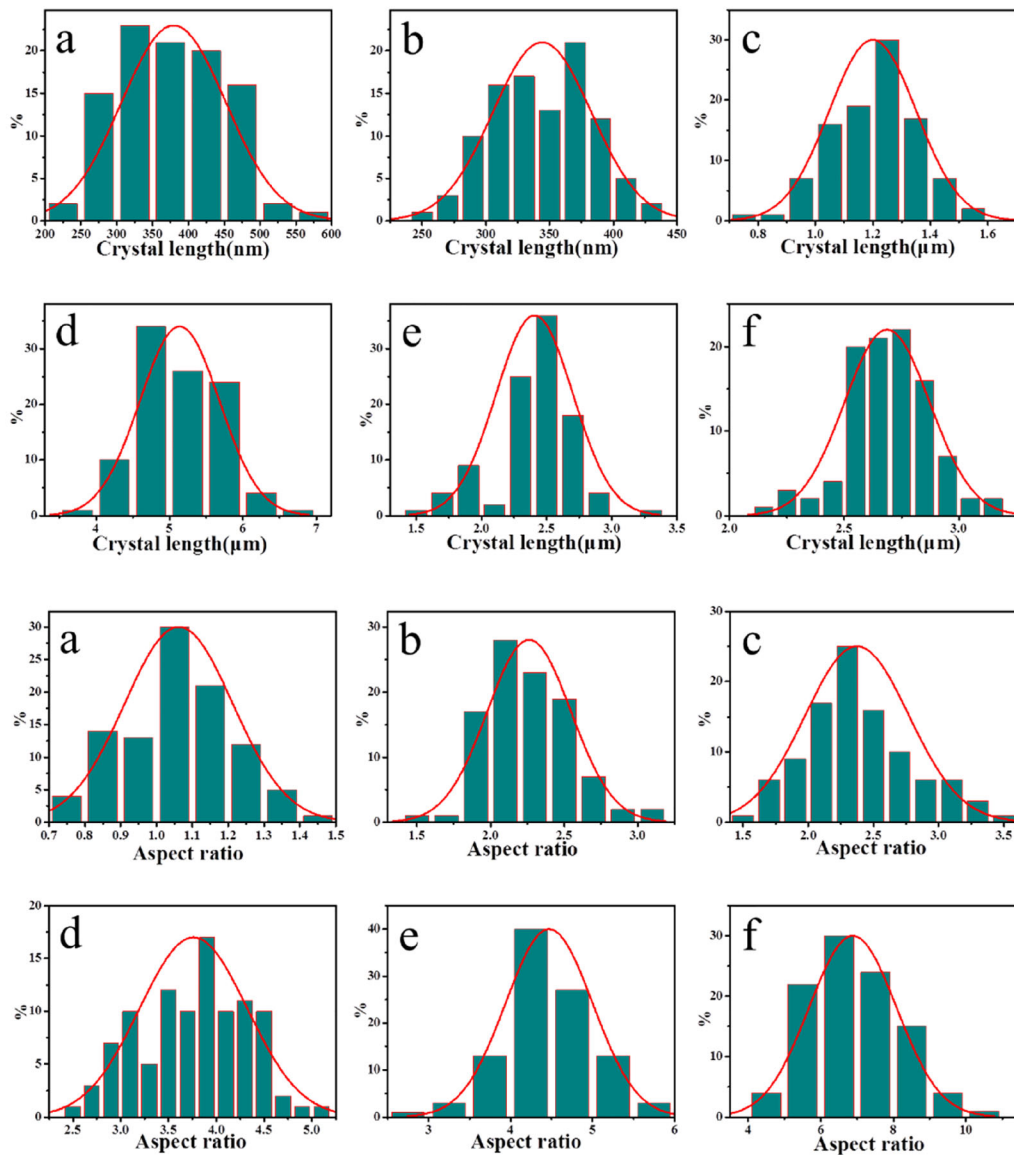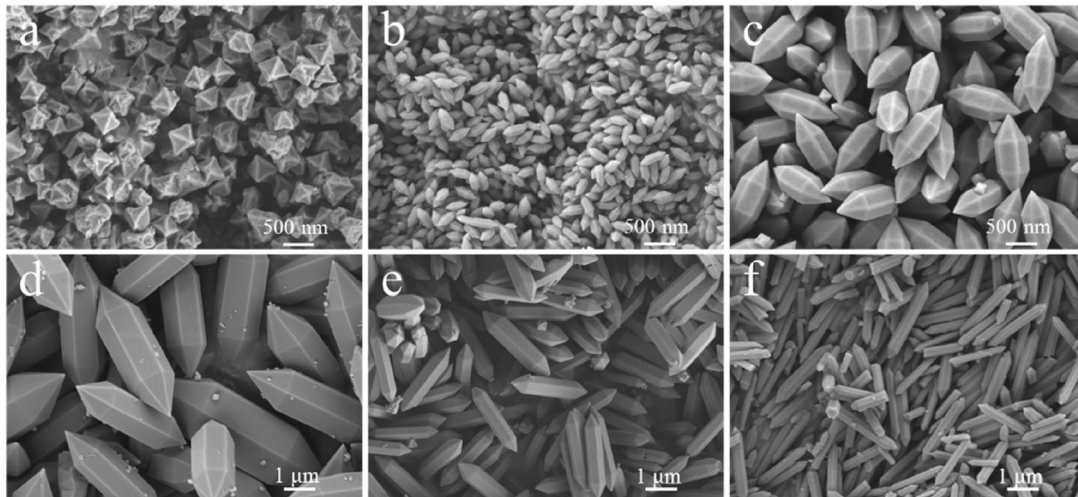
◀ **Fig. 3** The top, middle, and bottom panels present the SEM images, crystal length distribution, and aspect ratio distribution of NH$_2$-MIL-88B(Fe) crystals synthesized in DMF-water mixed solvents with different volume ratios of water: **a** 0 vol%, **b** 5 vol%, **c** 15 vol%, **d** 25 vol%, **e** 35 vol%, and **f** 45 vol%. 16 g PVP was added during the synthesis

range of 1.0–7.1. Over the water ratio range of 0–25 vol%, the crystal size increased dramatically, which is partially due to the effect of the PVP as a capping agent [24]; the average length increased from about 379 nm to about 5.14 μm and the average width increased from about 361 to 1.38 μm. However, as the ratio of water continued to increase to 45%, the size of the crystals decreased instead, with the average length and width of the crystals decreasing to 2.77 μm and 390 nm, respectively, but the aspect ratio of the crystals increased to as high as 7.1. This is likely because the interaction of the water molecules with the newly formed {011} crystal facets is much stronger than that with the {010} crystal facets. As the ratio of water in the mixed solvent increases, the influence of water molecules on the {011} crystal facets becomes stronger. The net effect is that the growth of the crystals along the [001] direction is inhibited and the average length of the crystals decreases. On the other hand, since both the water
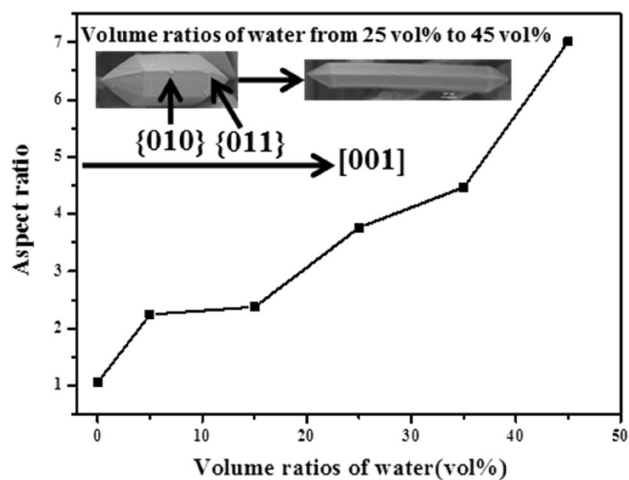
and the PVP have an effect on the growth of the {010} crystal facets, the width of the crystals decreases dramatically under their synergistic effects, which promotes the formation of nanorods with high aspect ratios. The evolution from spindle-like crystals with a relatively low aspect ratio to nanorods with a relatively high aspect ratio is clearly shown in the insert of Fig. 4.

Figure 5 shows the powder X-ray diffraction spectra of the same NH$_2$-MIL-88B(Fe) samples for which the SEM images are presented in Fig. 3. All the spectra show patterns expected for the NH$_2$-MIL-88B(Fe) structure [37]. As a reference, a simulated pattern of the Fe-MOF structure was built from the crystallographic information file (CIF) [43]. The diffraction peaks of all samples can match well with the peaks in the simulated XRD pattern of NH$_2$-MIL-88B, which demonstrates the successful preparation of Fe-MOF. There is a slight shift in the characteristic peaks in the XRD patterns of NH$_2$-MIL-88B(Fe) obtained by preparation in different solvents [44]. One can also see that the intensity of the (101) diffraction peak of the crystal increases with an increase in the ratio of water in the mixed solvent. This indicates that the higher the ratio of water in the solvent is, the higher the crystallinity of the sample is,
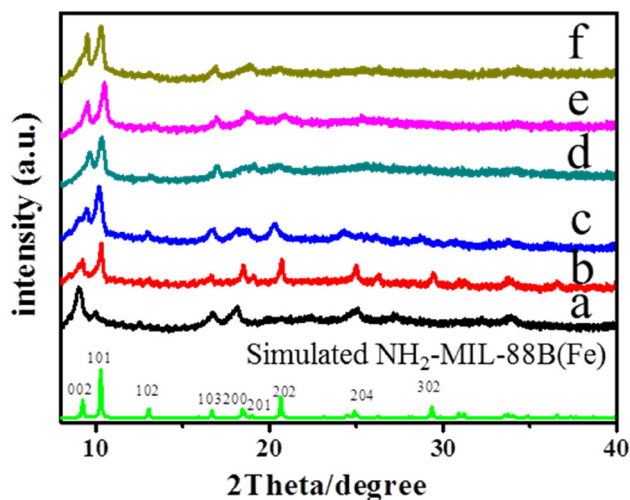

Fig. 4 The aspect ratio of NH$_2$-MIL-88B(Fe) crystals as a function of the volume ratio of water in the DMF-water mixed solvent. 16 g PVP was added during the preparation process. The insert shows the SEM images of a relatively short crystal and a relatively long crystal, which were prepared with the water ratios of 25 vol% and 45 vol%, respectively. The [001] direction and {010} and {011} planes of the crystals are indicated

Fig. 5 XRD patterns of NH$_2$-MIL-88B(Fe) crystals prepared with different volume fractions (x) of water in a mixed DMF-water solvent: (a) $x = 0$ vol%, (b) $x = 5$ vol%, (c) $x = 15$ vol%, (d) $x = 25$ vol%, (e) $x = 35$ vol%, and (f) $x = 45$ vol%. 16 g PVP surfactant was added during the synthesis. The green curve in the bottom of the figure is the XRD pattern simulated for the NH$_2$-MIL-88B(Fe) structure according to the CIF [43] (Color figure online)

which is consistent with the morphology evolution observed in the SEM images. The reason for this is that an increase in the ratio of water is beneficial to the formation of {101} crystal facets [45]. Table 2 gives the energy dispersive X-ray spectroscopy (EDS) data obtained on the same six samples for which the XRD patterns are presented in Fig. 5. The data confirm the composition of the NH_2-MIL-88B crystals, and the variations of the element percentages in different samples are within the ranges expected for the crystals.

3.4 Electromagnetic properties

The electromagnetic wave absorption performance of MIL-A was investigated. First, the relative permittivity ($\varepsilon_r = \varepsilon' - j\varepsilon''$) and relative permeability ($\mu_r = \mu' - j\mu''$) of a composite sample consisting of 25 wt% MIL-A and 75% wax were measured. Here, the real parts (ε' and μ') correspond to the storage capacity of electric and magnetic energy, while the imaginary parts (ε'' and μ'') represent energy dissipation. Figure 6a, b present the permittivity and permeability data, respectively. In each figure, the black and red dots show the real and imaginary parts, respectively. One can see that the values of ε' and μ' show an overall decreasing trend as the frequency increases, which means that the composites exhibit a typical frequency dispersion behavior. One can also see multiple resonance responses in the 8–18 GHz range, which may be attributed to polarization resonances.

The microwave absorption characteristics of sample MIL-A are presented in Fig. 7. The figure shows the microwave reflection coefficient calculated with the permittivity and permeability data presented in

Table 2 The EDS results of NH_2-MIL-88B(Fe) crystals synthesized in DMF-water mixed solvents with different volume ratios (x) of water

Element(Wt%)	a	b	c	d	e	f
C	48.46	51.71	53.65	61.77	53.32	52.12
N	26.63	25.65	19.45	15.39	20.56	22.45
O	23.06	20.52	24.63	20.73	23.78	23.14
Fe	1.85	2.12	2.27	2.11	2.34	2.29

a—x = 0 vol%, b—x = 5 vol%, c—x = 15 vol%, d—x = 25 vol%, e—x = 35 vol%, and f—x = 45 vol%. 16 g PVP was added during the synthesis

Fig. 6. According to the transmission line theory, the reflection coefficient or reflection loss (RL) of a layer of a material with a thickness d can be calculated as [39].

$$RL = 20l_g \left| \frac{(Z_{in} - Z_0)}{(Z_{in} + Z_0)} \right|, \tag{1}$$

where

$$Z_0 = \sqrt{\frac{\mu_0}{\varepsilon_0}}, \tag{2}$$

$$Z_{in} = Z_0 \sqrt{\frac{\mu_r}{\varepsilon_r}} \tan\left[j\frac{2\pi}{c} \sqrt{\mu_r \varepsilon_r} fd \right]. \tag{3}$$

Z_{in} and Z_0 stand for the input impedance of the material and the impedance of free space, respectively, f is the microwave frequency, and c denotes the speed of light. The calculations were carried out for four different thicknesses, as indicated in the figure. The horizontal dashed line in the figure indicates a RL of − 10 dB. This RL corresponds to a situation in which 90% of the microwave is attenuated in or absorbed by the material. Note that 90% absorption is expected for a material to be used as an absorber for practical applications [40]. One can see from Fig. 7 that the microwave absorbing performance of sample MIL-A has reached the standard of practical applications for a certain frequency range. For the thinnest case (d = 1.2 mm), the minimum RL at 15.7 GHz is -20 dB, and the effective absorption bandwidth (at − 10 dB) reaches 4.1 GHz. These data clearly show the potential of MOF crystals in this work for electromagnetic wave absorption applications.

4 Conclusions

By taking advantage of the synergistic effects of water and PVP surfactants, this work demonstrated the feasibility of a method for preparing NH_2-MIL-88B(Fe) crystals with both adjustable crystal size and aspect ratios and high uniformity. During the synthesis process, the amide unit of the PVP can be periodically coordinated with metal ions, which can stabilize the nucleation of MOFs during the crystal formation process and also promote a more uniform morphology. Water can significantly affect the deprotonation of ligand molecules during the synthesis process and
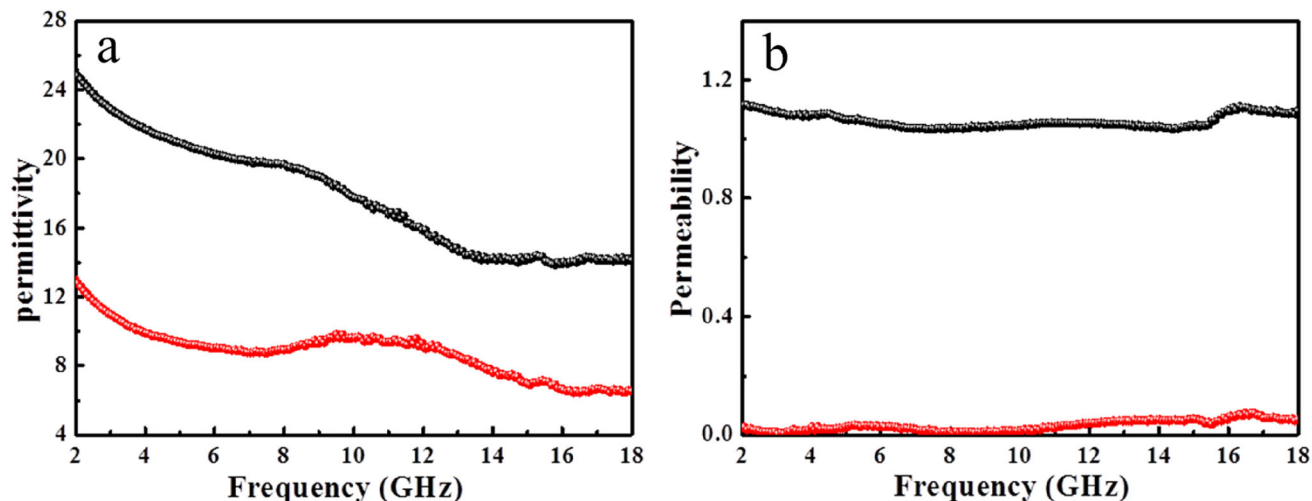
Fig. 6 a Relative permittivity and **b** relative permeability of sample MIL-A over a frequency range of 2–18 GHz. In each diagram, the black and red points show the real and imaginary parts, respectively (Color figure online)
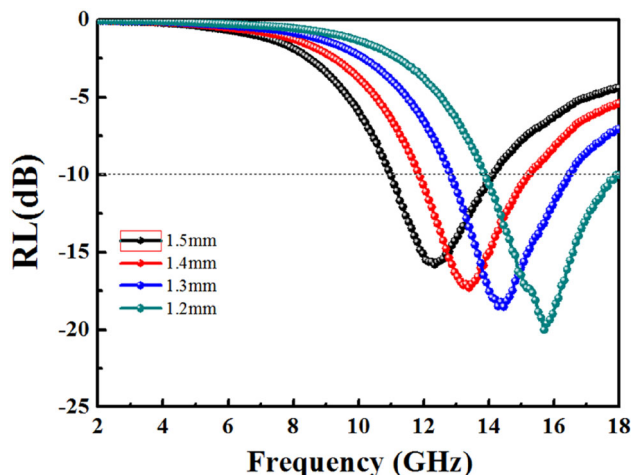

Fig. 7 RL of sample MIL-A with different thicknesses (1.5 mm, 1.4 mm, 1.3 mm and 1.2 mm). The horizontal dashed line indicates a RL of − 10 dB

thereby control the nucleation rate and the size of the crystals. Further, the PVP and water molecules play different roles in promoting the growth of certain crystal facets. Under their synergistic effects, the width of the crystals can be significantly reduced, promoting the formation of nanorods with high aspect ratios. In addition, the obtained sample with the highest aspect ratio was calcined at 800 °C, and this lightweight composite exhibits high potential for electromagnetic wave absorption applications; when the composite has a thickness of only 1.2 mm, the minimum reflection loss (RL) reaches is − 20.0 dB and the effective − 10 dB absorption bandwidth reaches 4.1 GHz. NH$_2$-MIL-88B(Fe) crystals with highly customizable size and

aspect ratios and high uniformity have potential applications in gas storage and separation, drug delivery, and electromagnetic wave absorptions.

Author contributions

JL: Conceptualization, methodology, validation, writing—original draft. JY: Formal analysis, investigation. SA: Investigation. MW: Formal analysis, investigation. XW: Data curation visualization, supervision. RG: Formal analysis, investigation, resources. YN: Validation, writing—review & editing, funding acquisition.

Funding

Data availability

The data that support the findings of this study are available from the corresponding author upon reasonable request.

Declarations

Conflict of interest The authors declare that they have no known competing financial interests or

personal relationships that could have appeared to influence the work reported in this paper.

References

1. O.M. Yaghi, G. Li, H. Li, Selective binding and removal of guests in a microporous metal–organic framework. Nature. **378**, 703–706 (1995)

2. N. Stock, S. Biswas, Synthesis of metal-organic frameworks (MOFs): routes to various MOF topologies, morphologies, and composites. Chem. Rev. **112**, 933–969 (2012)

3. L. Jin, Q. Liu, W. Sun, An introduction to synthesis and application of nanoscale metal–carboxylate coordination polymers. CrystEngComm **16**, 3816–3828 (2014)

4. A. Wei Xia, R. Mahmood, Q. Zou, Xu, Metal–organic frameworks and their derived nanostructures for electrochemical energy storage and conversion. Energ. Environ. Sci. **8**, 1837–1866 (2015)

5. Y. Cui, B. Li, H. He, W. Zhou, B. Chen, G. Qian, Metal–organic frameworks as platforms for functional materials. Accounts Chem. Res. **49**, 483–493 (2016)

6. A.H. Assen, Y. Belmabkhout, K. Adil, A. Lachehab, H. Hassoune, H. Aggarwal, Advances on CO2 storage. Synthetic porous solids, mineralization and alternative solutions. Chem. Eng. J. **419**, 129569 (2021)

7. D. Alezi, Y. Belmabkhout, M. Suyetin, P.M. Bhatt, Ł.J. Weseliński, V. Solovyeva, K. Adil, I. Spanopoulos, P.N. Trikalitis, A.-H. Emwas, M. Eddaoudi, MOF crystal chemistry paving the way to gas storage needs: aluminum-based soc-MOF for CH4, O2, and CO2 storage. J. Am. Chem. Soc. **137**, 13308–13318 (2015)

8. Y. Zhang, C. Wang, T. Zhu, P. Wang, S. Gao, Ultra-high uptake and selective adsorption of organic dyes with a novel polyoxomolybdate-based organic–inorganic hybrid compound. RSC Adv. **5**, 45688–45692 (2015)

9. X. Dai, Yu. Cao, X. Shi, X. Wang, The PLA/ZIF-8 nanocomposite membranes: the diameter and surface roughness adjustment by ZIF-8 nanoparticles, high wettability, improved mechanical property, and efficient oil/water separation. Adv. Mater. Interfaces **3**, 1600725 (2016)

10. B. Li, Y. Zhang, D. Ma, Lu. Li, G. Li, G. Li, Z. Shi, S. Feng, A strategy toward constructing a bifunctionalized MOF catalyst: post-synthetic modification of MOFs on organic ligands and coordinatively unsaturated metal sites. Chem. Commun. **48**, 6151–6153 (2012)

11. C.I. Ezugwu, B. Mousavi, M.A. Asrafa, A. Mehta, H. Vardhanab, F. Verpoort, An N-heterocyclic carbene based MOF catalyst for Sonogashira cross-coupling reaction. Catal. Sci. Technol. **6**, 2050–2054 (2016)

12. L. Gao, Q. Chen, T. Gong, J. Liu, C. Li, Recent advancement of imidazolate framework (ZIF-8) based nanoformulations for synergistictumor therapy. Nanoscale **11**, 21030–21045 (2019)

13. C. Sun, C. Qin, X. Wang, G. Yang, K. Shao, Y. Lan, Z. Su, P. Huang, C. Wang, E. Wang, Zeolitic imidazolate framework-8 as efficient pH-sensitive drug delivery vehicle. Dalton T **41**, 6906–6909 (2012)

14. C. Wang, H. Fu, P. Wang, C. Wang, Highly sensitive and selective detect of p-arsanilic acid with a new water-stable europium metal–organic framework. Appl. Organomet. Chem. **33**, e5021 (2019)

15. X. Zhang, G. Ji, W. Liu, B. Quan, X. Liang, C. Shang, Y. Chenga, Y. Du, Thermal conversion of an Fe3O4@ metal–organic framework: a new method for an efficient Fe–Co/nanoporous carbon microwave absorbing material. Nanoscale **7**, 12932–12942 (2015)

16. N.R. Sadegh Dehghani, S. Alam, T. Shahriarian, S. Mortezazadeh, A. Haghgoo, B. Golmohamadpour, M. Majidi, Khoobi, The effect of size and aspect ratio of Fe-MIL-88B-NH2 metal-organic frameworks on their relaxivity and contrast enhancement properties in MRI: in vitro and in vivo studies. J. Nanopart. Res. **20**, 1–16 (2018)

17. T. Rodenas, I. Luz, G. Prieto, B. Seoane, H. Miro, A. Corma, F. Kapteijn, F.X. Llabrés i Xamena, J. Gascon, Metal-organic framework nanosheets in polymer composite materials for gas separation. Nat. Mater. **14**, 48–55 (2015)

18. H. Vinh-Thang, S. Kaliaguine, Predictive models for mixed-matrix membrane performance: a review. Chem. Rev. **113**, 4980–5028 (2013)

19. Z. Lars Heinke, C. Gu, Wöll, The surface barrier phenomenon at the loading of metal-organic frameworks. Nat. Commun. **5**, 1–6 (2014)

20. T. Chalati, P. Horcajada, R. Gref, P. Couvreura, C. Serre, Optimisation of the synthesis of MOF nanoparticles made of flexible porous iron fumarate MIL-88A. J. Mater. Chem. **21**, 2220–2227 (2011)

21. P. Horcajada, T. Chalati, C. Serre, B. Gillet, C. Sebrie, T. Baati, J.F. Eubank, D. Heurtaux, P. Clayette, C. Kreuz, J. Chang, Y. KyuHwang, V. Marsaud, P.-N. Bories, L. Cynober, S. Gil, G. Férey, P. Couvreur, R. Gref, Porous metal–organic-framework nanoscale carriers as a potential platform for drug delivery and imaging. Nat. Mater. **9**, 172–178 (2010)

22. K.M.L. Taylor, A. Jin, W. Lin, Surfactant-assisted synthesis of nanoscale gadolinium metal-organic frameworks for potential multimodal imaging. Angew. Chem. Int. Edit. **47**, 7722–7725 (2008)

23. O. Friščić, D.G. Reid, I. Halasz, R.S. Stein, R.E. Dinnebier, M.J. Duer, Ion-and liquid-assisted grinding: improved mechanochemical synthesis of metal–organic frameworks

reveals salt inclusion and anion templating. Angew. Chem. **122**, 724–727 (2010)

24. X. Cai, J. Lin, M. Pang, Facile synthesis of highly uniform Fe-MIL-88B particles. Cryst. Growth Des. **16**, 3565–3568 (2016)

25. T. Tsuruoka, S. Furukawa, Y. Takashima, K. Yoshida, S. Isoda, S. Kitagawa, Nanoporous nanorods fabricated by coordination modulation and oriented attachment growth. Angew. Chem. **121**, 4833–4837 (2009)

26. J. Hwang, T. Heil, M. Antonietti, B.V.K.J. Schmidt, Morphogenesis of metal–organic mesocrystals mediated by double hydrophilic block copolymers. J. Am. Chem. Soc. **140**, 2947–2956 (2018)

27. X. Wang, S. Ma, D. Sun, S. Parkin, H. Zhou, A mesoporous metal—organic framework with permanent porosity. J. Am. Chem. Soc. **128**, 16474–16475 (2006)

28. Z. Zhao, H. Li, K. Zhao, L. Wang, Microwave-assisted synthesis of MOFs: rational design via numerical simulation. Chem. Eng. J. **428**, 131006 (2022)

29. L. Shao, Z. Yu, X. Li, X. Li, H. Zeng, X. Feng, Carbon nanodots anchored onto the metal-organic framework NH2-MIL-88B(Fe) as a novel visible light-driven photocatalyst: photocatalytic performance and mechanism investigation. Appl. Surf. Sci. **505**, 144616 (2020)

30. S. Yixuan Gao, Y.Y. He, Y. Fan, L. Zhang, J. Ma, R. Hou, L. Chen, J. Chen, A photo-fenton self-cleaning membrane based on NH2-MIL-88B(Fe) and graphene oxide to improve dye removal performance. J. Membrane Sci. **626**, 119192 (2021)

31. C. Hasirci, O. Karaagac, H.H. Kockar, Superparamagnetic zinc ferrite: a correlation between high magnetizations and nanoparticle sizes as a function of reaction time via hydrothermal process. J. Magn. Magn. Mater. **474**, 282–286 (2019)

32. F. Ozel, H. Kockar, S. Beyaz, O. Karaagac, T. Tanrisever, Superparamagnetic iron oxide nanoparticles: effect of iron oleate precursors obtained with a simple way. J. Mater. Sci. **24**(8), 3073–3080 (2013)

33. W. Zhao, J. Rong, W. Luo, L. Long, X. Yao, Enhancing the K-poisoning resistance of CeO2-SnO2 catalyst by hydrothermal method for NH3-SCR reaction. Appl. Surf. Sci. **579**, 152176 (2022)

34. Y. Bai Sun, W. Liu, J. Zhao, P. Wu, Chen, Hydrothermal preparation and white-light-controlled resistive switching behavior of BaWO4 nanospheres. Nano-Micro Lett. **7**(1), 80–85 (2015)

35. H. Bai Sun, L. Li, P. Wei, Chen, Hydrothermal synthesis and resistive switching behaviour of WO3/CoWO4 core–shell nanowires. CrystEngComm **16**(42), 9891–9895 (2014)

36. M. Takashi Uemura, S. Ohba, Kitagawa, Size and surface effects of Prussian blue nanoparticles protected by organic polymers. Inorg. Chem. **43**, 7339–7345 (2004)

37. M.-H. Pham, G.-T. Vuong, A.-T. Vu, D. Trong-On, Novel route to size-controlled Fe–MIL-88B–NH2 metal–organic framework nanocrystals. Langmuir **27**, 15261–15267 (2011)

38. X. Cheng, A. Zhang, K. Hou, M. Liu, Y. Wang, C. Song, G. Zhang, X. Guo, Size-and morphology-controlled NH2-MIL-53 (Al) prepared in DMF–water mixed solvents. Dalton **42**, 13698–13705 (2013)

39. J. Weihua Gu, B. Lv, X. Quan, B. Liang, G. Zhang, Ji, Achieving MOF-derived one-dimensional porous ZnO/C nanofiber with lightweight and enhanced microwave response by an electrospinning method. J. Alloy Compd. **806**, 983–991 (2019)

40. B. Zhang, J. Wang, J. Wang, S. Huo, B. Zhang, Y. Tang, Microwave absorption properties of lightweight absorber based on Fe50Ni50-coated poly (acrylonitrile) microspheres and reduced graphene oxide composites. J. Magn. Magn. Mate **413**, 81–88 (2016)

41. F. Chen, S. Zhang, B. Ma, Y. Xiong, H. Luo, Y. Cheng, X. Li, X. Wang, R. Gong, Bimetallic CoFe–MOF@ Ti3C2TxM-Xene derived composites for broadband microwave absorption. Chem. Eng. J. **431**, 134007 (2022)

42. T. Uemura, S. Kitagawa, Prussian blue nanoparticles protected by poly (vinylpyrrolidone). J. Am. Chem. Soc. **125**, 7814–7815 (2003)

43. S. Bauer, C. Serre, T. Devic, P. Horcajada, J.G. Marrot, N. Férey, Stock, High-throughput assisted rationalization of the formation of metal organic frameworks in the iron (III) aminoterephthalate solvothermal system. Inorg Chem. **47**(17), 7568–7576 (2008)

44. M. Ma, A. Bétard, I. Weber, N.S. Al-Hokbany, R.A. Fischer, N. Metzler-Nolte, Iron-based metal–organic frameworks MIL-88B and NH2-MIL-88B: high quality microwave synthesis and solvent-induced lattice "breathing." Cryst. Growth Des. **13**(6), 2286–2291 (2013)

45. C. Qiao, R. Zhang, Y. Wang, Q. Jia, X. Wang, Z. Yang, T. Xue, R. Ji, X. Cui, Z. Wang, Rabies virus-inspired metal-organic frameworks (MOFs) for Targeted imaging and chemotherapy of glioma. Angew. Chem. Int. **59**(39), 16982–16988 (2020)